Accepted Manuscript

Wear mechanism of spark plasma sintered MWCNTs reinforced zirconia composites under dry sliding conditions

Soukaina Lamnini, Csaba Balázsi, Katalin Balázsi

PII: S0043-1648(19)30440-5

DOI: https://doi.org/10.1016/j.wear.2019.05.020

Reference: WEA 102905

To appear in: *Wear*

Received Date: 4 March 2019

Revised Date: 19 May 2019

Accepted Date: 20 May 2019

Please cite this article as: S. Lamnini, C. Balázsi, K. Balázsi, Wear mechanism of spark plasma sintered MWCNTs reinforced zirconia composites under dry sliding conditions, *Wear* (2019), doi: https://doi.org/10.1016/j.wear.2019.05.020.

Wear mechanism of spark plasma sintered MWCNTs reinforced zirconia composites under dry sliding conditions

Soukaina Lamnini[a,b], Csaba Balázsi*[b], Katalin Balázsi[b]

[a]*Doctoral School of Material Science and Technologies, Óbuda University, Bécsi str.96/B, 1034 Budapest, Hungary*

[b]*Institute for Technical Physics and Materials Science, Centre for Energy Research, Hungarian Academy of Sciences, Konkoly – Thege M. str. 29-33, 1121 Budapest, Hungary*

**corresponding author: balazsi.csaba@energia.mta.hu*

Abstract

In this work multiwall carbon nanotubes (MWCNTs) reinforced 8 mol.% yttria-stabilized zirconia (8YSZ) composites were prepared using attrition milling and spark plasma sintering (SPS, at 1400 °C) in different compositions (0, 1, 5, 10 wt.% MWCNTs). The effect of sliding speed at low (V1= 0.036 m/s) and high (V2= 0.11 m/s) values has been investigated. Outstanding wear improvement at both low/high sliding speed has been reported with the addition of 1 wt.% of MWCNTs. This was most likely attributed to two main factors: 1) the formation of a perfectly continuous and uniform tribo-film. 2) the improved flexural strength, fracture toughness and density.

Keywords

8YSZ/MWCNTs composites, fractographic analysis, wear mechanism, tribological behavior, SEM/EDS.

Introduction

The optimization of wear resistance and friction coefficient is considered as a preliminary step during the design of a new tribological system, able to withstand sever thermo-mechanical environment. Reinforced ceramic composites appears nowadays commercially competitive to the traditional materials for example grey cast iron or carbon/carbon used in the fabrication of brake

systems which require optimised friction coefficient and high wear resistance [1,2]. In fact, nano-conductive particles, whiskers or fibres, multiwall carbon nanotubes (MWCNTs) or grapheme nano-platelets (GNP), multi-layered graphene (MLG) have been in several works endowed as a secondary phase into structural ceramics such as: yttria-stabilized zirconia (YSZ), silicon nitride (Si_3N_4), silicon carbide (SiC) or aluminum oxide (Al_2O_3) to improve their mechanical as well as tribological properties. The major advantages of reinforced structural ceramics reside in their greater strength, reduced density, high abrasion/wear resistance and high temperature stability [3]. Indeed, reinforced structural ceramics demonstrated high tribological performance at lab as well as industrial scale, which enable their wide commercialization for short and long operational life time applications. Advanced nozzle jet vanes used in missiles or hot structures for spacecraft are good examples of short life time applications where mostly melt infiltrated composites like C/C–SiC coated with a ceramic surface protection take a part [4]. Other typical applications requiring special wear resistance performances for longer structural lifetime are devoted to terrestrial applications including brake systems in cars, trains, aircraft or elevators. In this context, several ceramic matrix composites have been investigated for these purposes [2,5,6]. Kasperski *et al* [7] prepared MWCNT–ZrO_2 composites by spark plasma sintering. Several amounts of MWCNT (0.5, 1, 1.68, 3.24 and 5.16 wt.%) have been added to zirconia matrix. The wear test investigation has been performed under a load of 5 and 10 N using alumina ball as a counterpart. The frictional properties decreased with increasing MWCNT amount from 0.5 to 3.24 wt.%. However, the friction coefficient and the wear resistance were significantly improved with 5 wt.% MWCNT addition, which was in line with the softer track and the higher lubricating effect observed on the worn areas. On the other hand, the highest average arithmetic roughness was attributed to the composite with 5 wt.% of MWCNT about 0.11 μm compared to the other composites, where the roughness was in the range of 0.01-0.03 μm causing easier zirconia grains pull-out during polishing. Hvizdos *et al* [8] investigated the tribological properties of graphene nanoplatelets with 1 and 3 wt.% additions into Si_3N_4 matrix under (5 N) load and maximum sliding distance of 300 m. Steady-state of friction coefficient were recorded at short sliding distance followed by more or less higher fluctuation depending on the composite content. According to the results the composite with the best friction coefficient and wear resistance corresponded to 3 wt.% of graphene addition to Si_3N_4 matrix where the wear rate decreased by 60% compared to Si_3N_4 reference. The analysis of

microstructural features was related closely to the wear damage mechanism. In fact, it confirmed a strong graphene nanoplatelets interfacial bonding to silicon nitride matrix. This high integration of graphene nanoplatelets into the microstructure prohibited finding a significant lubrication effect during wear test. On the other hand, intensive milling process for more than 10 h played an important role to achieve efficient exfoliation and large distance between graphene multilayers and therefore acquire the expected tribological properties. Melk *et al* [9] studied the friction and wear behavior of spark plasma sintered 3 mol.% yttria-doped tetragonal zirconia (3Y-TZP) reinforced with up to 2 wt.% MWCNTs using zirconia ball with 10 mm diameter as a counterpart. In this study, the friction coefficients (COFs) were evaluated in macro-scratch testing with a sliding Rockwell indenter at increasing loads. Strong oscillations have been recorded in the COF beyond a critical load relatively higher. The oscillations appeared earlier for the composites with larger amount of MWCNT inducing brittle fracture and chipping trend. The origin of the brittle fracture and chipping were supposed to be resulted from the weak zirconia and MWCNTs interface or due to the tensile stresses appeared during the scratch test. However, the effect of MWCNTs addition on COF under low applied loads resided in considerable increases reflecting low wear rate. In another study, the influence of the applied load and sliding speed on the friction and wear behavior of ZrO_2 with 1.07 wt.% carbon nanofiber (CNFs) composite has been investigated by Hvizdos *et al* [10]. A slight variation of the friction coefficient (0.22–0.27) for various sliding speeds 2.5, 5, 10, 15 $cm{\cdot}s^{-1}$has been found. In addition, a significant increase in the friction coefficient with respect to the applied load from (0.25 to 0.35 via 1 N to5 N) respectively has been observed. A low amount of debris formed by (CNFs) and zirconia particles appeared at (1 N) applied load. However, at higher load (5 N) zirconia grains and perpendicularly oriented CNFs pull-out to the worn surface were observed. In fact, the mixture formed a transferred film which led to attain a lubricating effect during sliding and therefore enhanced the tribological properties of the composite.

In this study, we have focused on studying the tribological performance of 8YSZ/MWCNTs composites with the aim of providing a better understanding of tribo-film formation mechanism with respect to MWCNTs content and sliding speed during the wear test. Based on the well understanding of the wear mechanism, the further objective of this study is to enable the technological maturation of ceramic– MWCNTs composites in the future.

Experimental procedure

Commercial 8 mol.% yttria-stabilized zirconia powders (8YSZ, Sulzer Metco AMDRY 6643) with cubic crystal lattice as main structural phase and minor proportion of monoclinic phase were used in the study. The average grain size of the as-received zirconia powder is about 40 µm. MWCNTs (type NC3100™, Nanocyl) with an average walls number of eight and inner/outer diameterof 3.8 nm/9.13 nm, respectively were added to zirconia powder with 1 wt.%, 5 wt.% and 10 wt.%. The composite mixtures were milled in wet media (ethanol) for 5 h and 4000 rpm using attritor milling (Union Process, type 01-HD/HDDM) and zirconia balls (1 mm in diameter). The composites in powder state had been dried at 172 °C for 25 minutes and sieved with a filter with mesh size of 100 m. The consolidation of the composites sized of 30 mm in diameter and 5 mm in thickness was assessed by SPS (SPS, HD P5 equipment FCT GmbH) at 1400 °C under vacuum (1mbar) and uniaxial pressure of 50 MPa maintained during a dwell time of 5 min. Intensive polishing with silicon carbide papers from 80 µm to 1200 µm has been applied on the sintered pellets in order to well remove the graphite paper traces used during sintering process and to reveal the composites microstructure. The final materials were shaped into bars sized of (4.8 mm × 4.4 mm × 30 mm) by diamond cutting (Struers Secotom-50). The apparent density (ρ) was evaluated using Archimedes principle for the composites with high and low porosity. The hardness (H_v) was evaluated from the diagonal length of the indentation marked by Vickers indenter (Shimadzu HMV 2000) at 19.61 N load, dwell of time of 30 s for each polished composites and calculated according to equation 1:

$$H_v = \frac{189.F.10^3}{d^2} \quad (1)$$

Where, F is the applied load (N) and d is the diagonal length (mm).

Semi-circular crack systems formula given by Shetty [11] was used to determine the indentation fracture toughness based on the propagated crack length. The composites were bended using 3-point bending apparatus (INSTRON5966) with span of 20 mm. Friction tests were carried out on High Temperature Tribometer THT (CSM, Switzerland) using ball-on-disk technique at room temperature (25 °C, air humidity 50–65%).

Commercially available Si_3N_4 balls with 5 mm in diameter, $H_{v\ 10}$ = 1300 N/mm² in hardness and Ra = 0.025 μm in roughness, were used as counterparts against the sintered 8YSZ and MWCNT/8YSZ composites. The friction coefficient (μ) has been recorded throughout the test with acquisition rate of 5.4 Hz at fixed normal load (5 N) and total sliding distance of d = 400 m. The speed velocity has been set up at V1= 0.036 m/s then V2= 0.11 m/s to study its influence on tribo-film formation and friction behaviour. The wear track profile and damage were characterized and analysed by Scanning Electron Microscopy (SEM, Thermo Scientific, Scios 2) as well as Digital Microscope (KEYENCE, VHX-950F).

Energy dispersive X-ray spectroscopy (EDS, Oxford X-Maxdetector with Aztec software) was performed for elemental identification inside and outside the wear track. Additional characterization of the wear mechanism based on average arithmetic roughness (Ra) measurements on the worn surfaces was performed with Digital Microscope (KEYENCE, VHX-950F).

The wear rates (W) were measured based on the volume loss (V) per total sliding distance (d) according to the following equation:

$$W = \frac{V}{d}\left[\frac{mm^3}{m}\right] \tag{2}$$

3. Results and discussion

3.1 Microstructure and mechanical properties of 8YSZ/MWCNT composites

SEM analysis is used to quantify the micro structural properties of 8YSZ composite with different amount of MWCNTs (0 wt.%, 1 wt.%, 5 wt.% and 10 wt.%) after fractographic test as illustrated in Fig. 1. SEM micrographs of the well milled monolithic zirconia (ZR, Fig. 1a) revealed a coarse microstructure with an average grain size of approximately 6.11 ± 4.08 μm, which is significantly higher than the recorded ones with added MWCNTs. Subsequently, as presented in Table 1 a drastic reduction of the grain size has been observed in the structure of ZR-1 composite from 6.11 ± 4.08 μm to 0.96 ± 0.49 μm. At the same time, according to Fig. 1b it can be clearly seen that the grains appear mostly plate shaped and sharp at edges reflecting

well pinned MWCNTs along the grain boundaries. Hence, the well dispersed MWCNTs led the formation of an extra barrier to fracture propagation along the grain boundaries. This behaviour is reinforced by minimal apparent porosity (16.50 %) obtained in this composite (ZR-1).

As consequence, high amount of fracture energy is required to propagate into the next neighbor grain, which led to a considerable flexural strength displayed by transgranular fracture mode as a dominant mechanism. By contrast, obvious microstructural transformation induced by increasing MWCNTs is observed in ZR-5 and ZR-10 composites as shown by SEM micrographs in Fig.1c and Fig.1d respectively. Furthermore, the microstructural modification was illustrated mainly by severe grain refinement $0.54 \pm 0.04\ \mu m$ in ZR-5 composite and $0.28 \pm 0.01\ \mu m$ in ZR-10 composite, simultaneously with the observation of a considerable increase in the residual porosity to 41.64 % via ZR-5 and to 46.28 % via ZR-10 resulting from inevitable agglomeration of higher amount of MWCNTs in matrix.

Indeed, despite the high sintering temperature of 1400 °C used during the composites consolidation process, the higher amount of MWCNTs inhibits grain growth and favorite's intergranular fracture mode occurrence especially for ZR-5 and ZR-10 composites. The arrows of dashed line marked in Fig.1c/d show a significant random dispersion of MWCNTs along the grain boundaries within the fine and granular microstructure, suggesting relatively weak surface bonding and easier fracture propagation along the weakest areas (grain boundaries) rather than through the grains, therefore intergranular fracture mode is more remarkable in ZR-5 and ZR-10 composites.

On the other hand, various possible directions of MWCNTs besides the perpendicular direction to sintering pressureis claimed to be possible with an optimum amount added to the matrix. More importantly, diverse directions of MWCNTs are among the principal key factors responsible of toughening mechanismsin YSZ/MWCNTs composites (like crack deflection, bridging and branching) as have been reported in the literature [12]. Furthermore, Declan *et al* [13] have investigated the influence of second phase features inclusion into ceramics matrix on toughening mechanism. The dominance of crack deflection was observed when the modulus of the second phase was increasing resulting in considerable strength enhancement.

The mechanical and structural properties of all the specimens are summarized in Table 1. Three-point bending test was carried out at room temperature for all the specimens. The flexural

strength shows an increase in favour of ZR-1 compared to the monolithic material (ZR) from 464 MPa to 502 MPa. Meanwhile, ZR-5 and ZR-10 express typical brittle fracture confirmed by critical decline of the flexural strength to 263 MPa and 166 MPa respectively, which is very consistent with the previously SEM micrographs analysis. The measured apparent density ρ follows similar behavior as the flexural strength varying between a maximum and a minimum of 6.75/4.36 g/cm^3 respectively. The calculated hardness values shown in (Table 1, Hv) are the average of seven indents measured on the specimen's diagonal with 4 mm displacement. Higher hardness values were achieved in both ZR composite equal to 13.49 ± 0.23 GPa and ZR-1composite of about 12.44 ± 0.97 GPa compared to similar composition and testing conditions [9,14]. However, in case of ZR-5 and ZR-10 the average hardness dropped to low values, confirming the influence of high MWCNTs content on the overall strength of ceramic composites [15,16]. The average fracture toughness *Kc* obtained along the specimen's surfaces with different MWCNTs content using indentation crack length size are also presented in (Table 1, *Kc*). In the present work, the reported fracture toughness *Kc* of the monolithic material ZR (3.06 ± 0.22) MPa·m$^{1/2}$ was slightly higher than ZR-1 (2.63 ± 0.62) MPa·m$^{1/2}$ composite. It is worth noting that, the latter manifested a fluctuated tendency along the tested surface diagonal, where in some positions a slight improvement was obtained [17]. Hence, this can be mainly attributed to well dispersion of MWCNTs along the gains boundaries after high sintering temperature (1400 °C). In our case the *Kc* decreased further by increase of MWCNTs addition, the ZR-5 and ZR-10 presented 1.28 ± 0.42 MPa·m$^{1/2}$ or 1.30 ± 0.44 MPa·m$^{1/2}$ (Table 1). In the same context, Melk *et al* [15] studied (3Y-TZP) composites with 0–2 wt.% MWCNTs content with grain size in the range of 177-148 nm, then compared their fracture toughness obtained via single edge V-notch beam (SEVNB) and via indentation size induced by Vickers indenter. As a results, the fracture toughness obtained via indentation increased with MWCNTs content and show relatively higher values in the range of (3.57– 4.97) MPa·m$^{1/2}$, while the true fracture toughness measured using SEVNB varied independently of the composition, and manifested lower values about (2.8 MPa·m$^{1/2}$). In a relatively similar finding [14] Mazaheri *et al*, reported higher fracture toughness using indentation method compared to single edge V-notch bean (SEVNB) technique. However, to the best of our knowledge both methods led to obtain the highest fracture toughness value of (10.9 ± 0.42MPa·m$^{1/2}$) cited in the literature when increasing MWCNTs content to 5 wt.%.

The controversial results of toughness data reported by several authors under similar composition and processing methods, draw clearly the importance to make compromises between accuracy, time consummation and the complexity of the experimental procedure with regard to microstructural features of the composites such as (grain size and effective crack lengths) while choosing the fracture toughness testing method as discussed in detail elsewhere [18–20]. Therefore, the reliability and suitability of the empirical relationships and different testing techniques must be carefully taken into consideration during the interpretation of the final results devoted to tribological investigation.

Table 1

Fig. 1

3.2 Average Friction coefficient (μ) and wear rate (W)

The average friction coefficient (μ) corresponding to the sliding distance in the range of 0–40 m and 40–400 m of the sintered composites tested under V1= 0.036 m/s, V2= 0.11 m/s sliding speeds, using ball on disc method and Si_3N_4 balls counterpart are presented in Fig. 2. Generally, the steady state friction coefficient (μ_{AFS}) is attained from ~ 40 m of sliding distance in all the composites. Its average values are presented in Fig. 2. At low sliding speed (V1= 0.036 m/s) the average steady state friction coefficient (μ_{AFS}) is seen to be significantly high~0.76 and quit similar to all the tested composites regardless their specific micro-structural properties or MWCNTs content. However, the tribo-test carried out at V2= 0.11 m/s sliding speed reveals the existence of proportional relationship between the average steady state friction coefficient (μ_{AFS}) and the mechanical properties evolution as well as grain size. In fact, this relationship is manifested by decrease in (μ_{AFS}) regarding the more brittle composites possessing lower grain size as well as mechanical properties (0.608 via ZR-5 and 0.649 via ZR-10). Whereas, ZR and ZR-1 composites owing higher grain size and particular mechanical properties characterized majorly by transgranular fracture mode, the steady state friction coefficients (μ_{AFS}) recorded at high sliding speed V2 (0.777 via ZR and 0.726 via ZR-1) were found to be quite high and similar to the obtained ones at lower sliding speed.

Fig. 2

The wear rate results performed on the surface of 8YSZ-MWCNTs composites at both sliding speeds are illustrated with the red and black curves as presented in Fig. 3. According to this figure ZR composite exhibits an obvious sever wear behavior confirmed by its highest wear rate of about (5.55×10^{-3} mm^3/m) recorded at V1 sliding speed. A contrasting trend is marked in ZR-1 composite, where a fascinating improvement of the wear rate was established at low speed V1 (4.73×10^{-6} mm^3/m) exceeding all the other composites. This tendency is attributed in fact to its highest flexural strength and apparent density (ρ= 6.75 g/cm^3). Furthermore, at the same speed quantitatively significant low wear rate is also well recognised with the addition of 5 wt.% MWCNTs, this value is seen to increase slightly in ZR-10 composite but remains still lower compared to the severe wear observed in the monolithic material (ZR). Applying high velocity (V2= 0.11m/s) resulted in a better wear resistance. In fact, the wear rate results were closely similar or occasionally high in all the composites, therefore the influence of structural properties was not recognized as MWCNTs content increased. Comparative view between Fig. 2 and Fig. 3 sign a particular similar decreasing tendency of the wear rate and steady state friction coefficient (μ_{AFS}) in ZR-5 and ZR-10 composites as the speed increase. This is obviously linked to the previous microstructural evolution due to MWCNTs content increase as reported previously.

Fig. 3

According to the current study we deduce that grain size, density, mechanical properties or even sliding speed play a major role to beneficially or adversely affect the tribological performance of the structural ceramic composites. Indeed, these parameters vary dependently to MWCNTs content in the matrix, where high content led to a huge grain refinement and an obvious lubricant effect at the contacts areas between ball/surface, which decreases the friction coefficient. Therefore, it can be concluded that MWCNTs plays an indirect factor influencing the overall tribological behaviour of the composites. In addition, another important factor which mostly reflects a direct insight into friction behaviour consists in the evaluation of the average arithmetic surface roughness (Ra) of the composites inside the wear track after tribo-test at both sliding speed. In similar context, Nieto *et al* [21] reported an inversely proportional relationship (at high GNP content) between the applied load and surface roughness. The latter, is supposed to increase with

the friction and vice-versa. However, in their work the effect of surface roughness on friction behaviour was not evaluated with respect to sliding speed variation. Quite similar approach is developed in the current study but at increased sliding speed instead of applied load variation. The corresponding results shown in Table 2 reveal a remarkable decrease of Ra from 1.5 to 0.2 μm in ZR-5 and from 0.7 to 0.2 μm in ZR-10 when the sliding speed increased to V2. Therefore, applying high sliding velocity can be considered as another key factor also inversely proportional to the roughness of YSZ/MWCNTs composites extensively at high content. On the other hand, the measured roughness inside the wear track of ZR decreased only by 0.1 µm from its initial value after polishing process (0.6 µm) at low sliding speed V1. Additionally, slightly higher roughness decrease was also noticed in ZR-1 from 0.6 µm to 0.3 µm, which match well with the proportional high friction tendency obtained in these two composites (ZR, ZR-1) at V1 speed. However, the fine roughness values found in ZR-5 and ZR-10 tested at V2 were systematically increased inside the wear track at lower speed V1. This can be attributed to surface fluctuation induced by agglomeration of MWCNTs which could not be suppressed at low sliding speed. Here again, the measured values of the roughness are in good agreement with the low friction response delineated in Fig. 2.

Table 2

Wear (W) damage mechanism

The wear mechanism and the induced damage remained after tribo-test carried out at V1 and V2 speed were assessed using SEM measurements as presented in Fig. 4. According to the previous results presented in Fig. 2 and Fig. 3, ZR composite manifested high steady state friction coefficient (μ_{AFS}) as well as high wear rate at low sliding speed V1. This behavior is effectively shown to be very coherent with the morphological features inside the wear track profile shown in SEM micrograph (Fig. 4a). Indeed, the micrograph illustrates clearly the formation of a fractured ultra-thin tribo-film which appears almost incomplete and abrasively damaged during the tribo-test. Furthermore, zirconia grain pull-outs, delaminated areas, micro cracks and highly wear debris content are observed on the wear track profile and supposed to act as a main possible wear mechanism in the monolithic material. In fact, the wear debris resulting from tribo-film fracturing is assumed to react as a third body abrasive particle between the rubbing surfaces, leading to a significant rise in the friction

and wear rate. Moreover, the high wear rate obtained in ZR at V1 sliding speed can be assigned to it large grain size (6.11± 4.08) μm with a plate shape and to the dry sliding condition, therefore affording high friction behavior. More importantly, the difference in the mechanical properties of phase composition is highly believed to act as another key factor, which can entail stress concentrators and creates abrasive grooves on the worn area as depicted in SEM micrographs of ZR composite tested at high sliding speed V2 (Fig. 4e). In this context, the phase composition of all the tested composites before and after sintering and its influence on the overall mechanical properties are largely investigated elsewhere [17,22]. In addition, residual abrasives grooves might also come from primarily surface polishing process. In the case of ZR-1 composite, a perfectly continuous and uniform tribo-film was formed during the test at both sliding speeds (V1 as well as V2) as shown in Fig. 4b and f respectively. Further, it can be clearly seen that neither severe film fragmentations nor wear debris or micro cracks are observed within the wear track, but only minor plastic flows and light pits. Indeed, the high wear performance manifested in ZR-1 corresponds principally to MWCNTs-induced toughening mechanism and the creation of a protective thin tribo-film. MWCNTs-induced toughening mechanism influenced the wear performance of our material by dissipating energy through deformation, crack bridging, crack branching and crack deflection. These mechanisms restrain cracking on both the track surface and sub-surface. The existence of these toughening mechanisms were confirmed and well explained in our previous work [17]. Similar observations have been obtained by Li et al. [23] during the wear test of ZrO_2–GNP composites. On the other hand, the granular structure of ZR-5 composites tested at V1 sliding speed inhibited the formation of continuous tribo-film as seen in Fig. 4c where only tick (islands) are observed besides severe peeling that cause surface removal on the track. This specific behavior is attributed to the increased agglomeration of MWCNTs and the superficial porosity which could not be suppressed under the applied load and low speed. Zhang et al. [24] have reported similar observations with graphene nano-platelet (GNP)-reinforced aluminum oxide (Al_2O_3) composites. However, in the current study MWCNTs pull-out were also noticed in some areas of the wear track (Fig. 4c), which is acting as an intrinsic lubricant suggesting the reported improvement in the wear rate. In case of ZR-10 the formed tribo-layer appears more or less coherent. However, some delaminated areas, wear debris and micro-cracks were also observed masking the obtained slight wear rate increase in this composite compared to ZR-5. On the other hand, the

combined effect of applied load and high speed V2 were beneficial to enable the formation of dense, smooth and continuous lubricant areas on the worn surface of ZR-5 and ZR-10 composites as seen in Fig. 4j and Fig. 4h respectively. Additionally, under load of 5 N the small and rounded particles with a size of about 0.54 and 0.28 μm respectively were expected to coalesce easily in the asperity valleys, which systematically diminish the superficial porosity and thereby permit the typical established improvement in friction and wear. It would be more interesting to examine the morphology of the wear track profile and the previously discussed wear mechanism characterizing the composites separately at higher magnification. For this reason, we present in Fig. 5 and Fig. 6 the Keyence images employed on the wear tracks at both sliding speeds V1 and V2 respectively. From the images its shown an obvious increase in the width of the wear track simultaneously with MWCNT content. The abrasive wear mechanism and amount of wear debris manifested in ZR composite at low sliding speed is confirmed by Fig. 5a.

Fig. 4

Fig. 5

Fig. 6

3.3Chemical composition inside/outside the wear track of 8YSZ/MWCNT composites examined by EDS spectroscopy

In order to identify the microstructural evolution and correlated with the observed wear mechanisms mainly from chemical point of view, EDS analysis was employed inside the worn and unworn surfaces of 8YSZ and 8YSZ/MWCNTs composites as represented in Fig. 7. The analysis of EDS spectra conducted mainly to the following results: (Zr) peak is observed to decrease significantly during the fiction test performed at low speed in ZR composite while, the intensity of (O) remained practically identical. In fact, the high hardness and large grain size enable to the matrix to support more of the contact load during surface rubbing (ball/composite). This led in turn to high abrasion in (Zr) particles. As consequence, the latter undergoes severe pull out followed by scattering along the worn and unworn track profile to form wear debris as seen in the previous corresponding SEM micrograph. As a result, the

intensity of (Zr) element decreased sharply as seen in Fig. 7 accompanied with high wear and friction response. Contrasting chemical composition tendency is recognized at high speed for ZR composite (Fig. 7e). Thus, it's highly believed that de-bounding between (O) and (Zr) atoms occurred in the monolithic material tested at high speed, manifested by high increase in (O) peak and slight decrease in (Zr) peak inside the wear track, accompanied with appearance of (Si) peak. The decreased (Zr) peak intensity is attributed to the possibility of zirconium atoms scatted outside the track, while the (O) atoms resulted from de-bounding remained inside the track to cluster with (Si) transferred from the counterpart and therefore enhance the formation of thick SiO_2 layer that which improve the wear performance.

In ZR-1 composite the presence of (Si) peak after tribo-test is confirmed by EDS spectra (Fig. 7b) despite the low sliding speed. Eventually, in this case neither the matrix (zirconia) nor MWCNTs have experienced sever abrasive wear, this is well validated by the observation of minor decrease of (Zr) which systematically induced as light increase of (O) peak due to zirconia de-bounding mechanism. From structural view of carbon, non-remarkable damage is expected to occur after friction test as confirmed by the unreduced intensity of (C) peak. As consequence, the formed tribo-layer at V1 consists mainly of (Si) particles and minor fraction of (O). These results are in good agreement with SEM investigation showing the formation of a perfectly continuous and uniform tribo-film without any remarkable surface damage. Similar peak tendency is approved with increasing speed, however (Si) and (O) become more intense and therefore (Zr) peak lowered due to de-bounding mechanism.

EDS analysis shows highly dissimilar behavior between the group of (ZR, ZR-1) and (ZR-5, ZR-10) composites. Indeed, the intensities of (Si) and (O) peaks are recorded to increase simultaneously with MWCNTs content till attending its highest values in ZR-10 at V1 (approximately of three times inside the track). Furthermore, (Si) peaks corresponding to the group of (ZR, ZR-1) were intensified essentially by the increase of sliding speed. More importantly, the main difference clearly displayed in the spectra of ZR-5 and ZR-10 compared to ZR and ZR-1 consists in a sharp decrease of (C) peak intensity obtained inside the worn surface. This is supposed to be linked with MWCNTs exfoliation, giving rise to appreciable lubricant effect. In fact, from the spectra displayed in (Fig. 7j) it's well noted that ZR-5 composites

manifested the largest decrease of (C) peak after tribo-test justifying the improved friction response at high sliding speed.

On the other hand, besides the observed lubricant effect due to MWCNTs exfoliation, the friction decrease in ZR-10 at high sliding speed is thought to be the result of the high Si particles transfer from the counterpart to the surface and its adherence to (O) resulted from the easier YSZ matrix de-bounding under friction test. In addition, despite the high increase of (O) peak intensity and contrary to monolithic material, (Zr) peak is increased slightly suggesting less scattering of zirconium particles to form wear debris but were instead induced into the so-formed SiO_2 layer giving rise to compacted and dense areas in the tribo-layer of ZR-10.

Conclusion

8YSZ composites with (0 wt.%, 1 wt.%, 5 wt.% and 10 wt.%) of MWCNTs contents were synthesized by attrition milling and SPS at 1400 °C. The tribological properties of the composites have been investigated using Si_3N_4 balls, low (V1= 0.036 m/s), high (V2= 0.11 m/s) sliding speed and dry sliding conditions. At the speed of V1= 0.036 m/s, 8YSZ− 1 wt.% MWCNTs exhibited 99.9 % improvement in the wear rate followed by 95 % in 8YSZ−5 wt.% MWCNTs and 64% in 8YSZ− 10 wt.% MWCNTs composite compared to pure 8YSZ. Furthermore, the observation of grain pull-outs, micro cracks and high amount wear debris in pure 8YSZ give the evidence of abrasives wear behavior as main wear mechanism. This is shown to be linked with its coarse microstructure and the dry sliding condition. The outstanding wear improvement marked in 8YSZ−1 wt.% MWCNTs is in good agreement with the formation of continuous and uniform tribofilm on the worn surface. However, at 10 wt.% of MWCNTs content the tribofilm is discontinuous and does not protect from the brittle fracture due to the structural defects such as agglomeration and porosity. At the speed of V2= 0.11 m/s, minimal wear rate values have been recorded in all the composites regardless MWCNTs content. Further, the steady state friction coefficient decreased in the case of 8YSZ−5 wt.% MWCNTs and 8YSZ− 10 wt.% MWCNTs composites, reflecting easier sliding between the rubbing surfaces and friction improvement. In fact, this friction improvement is shown to be linked with the apparition

of intrinsic solid lubricant effect due to MWCNTs exfoliation (carbon peak decrease) and Si incorporation as confirmed by EDS spectrum.

Acknowledgement

The authors would like to thank gratefully Dr. György Zoltán Radnóczi and Mr. Tamás Zagyva for their technical assistance during EDS, Keyence microscope measurements and to Dr. Zoltán Károly for sintering of samples respectively. The authors acknowledge the support given by the Hungarian National Research Development and Innovation Office for the funding of FLAG-ERA, NKFIH NN 127723 "Multifunctional Ceramic/Graphene Coatings for New Emerging Applications"and NKFIH-NNE 129976 projects.

References

[1] Krupka M, Kienzle A. Fiber reinforced ceramic composite for brake discs. 18th Ann Brake Colloq Eng Disp 2000. doi:10.4271/2000-01-2761.

[2] Krenkel BW, Heidenreich B, Renz R. C / C-SiC Composites for Advanced Friction Systems 2002:427–36.

[3] Surappa MK. Aluminium matrix composites: Challenges and opportunities. Sadhana - Acad Proc Eng Sci 2003;28:319–34. doi:10.1007/BF02717141.

[4] Krenkel W, Berndt F. C/C-SiC composites for space applications and advanced friction systems. Mater Sci Eng A 2005;412:177–81. doi:10.1016/j.msea.2005.08.204.

[5] Liang Y, Dutta SP. Application trend in advanced ceramic technologies. Technovation 2001;21:61–5. doi:10.1016/S0166-4972(00)00019-5.

[6] Chapman TR, Niesz DE, Fox RT, Fawcett T. Wear-resistant aluminum-boron-carbide cermets for automotive brake applications. Wear 1999;236:81–7. doi:10.1016/S0043-1648(99)00259-8.

[7] Kasperski A, Weibel A, Alkattan D, Estournès C, Turq V, Laurent C, et al. Microhardness and friction coefficient of multi-walled carbon nanotube-yttria-stabilized ZrO_2 composites prepared by spark plasma sintering. Scr Mater 2013;69:338–41.

doi:10.1016/j.scriptamat.2013.05.015.

[8] Hvizdoš P, Dusza J, Balázsi C. Tribological properties of Si_3N_4-graphene nanocomposites. J Eur Ceram Soc 2013;33:2359–64. doi:10.1016/j.jeurceramsoc.2013.03.035.

[9] Melk L, Rovira JJR, Antti ML, Anglada M. Coefficient of friction and wear resistance of zirconia-MWCNTs composites. Ceram Int 2014;41:459–68. doi:10.1016/j.ceramint.2014.08.092.

[10] Hvizdoš P, Puchý V, Duszová A, Dusza J. Tribological behavior of carbon nanofiber-zirconia composite. Scr Mater 2010;63:254–7. doi:10.1016/j.scriptamat.2010.03.069.

[11] Shetty DK, Wright IG, Mincer PN, Clauer AH. Indentation fracture of WC-Co cermets. J Mater Sci 1985;20:1873–82. doi:10.1007/BF00555296.

[12] Cui E, Zhao J, Wang X, Sun J, Huang X, Wang C. Microstructure and toughening mechanisms of Al_2O_3/(W, Ti)C/graphene composite ceramic tool material. Ceram Int 2018;44:13538–43. doi:10.1016/j.ceramint.2018.04.185.

[13] McNamara D, Alveen P, Carolan D, Murphy N, Ivanković A. Micromechanical Study of Strength and Toughness of Advanced Ceramics. Procedia Mater Sci 2014;3:1810–5. doi:10.1016/j.mspro.2014.06.292.

[14] Mazaheri M, Mari D, Schaller R, Bonnefont G, Fantozzi G. Processing of yttria stabilized zirconia reinforced with multi-walled carbon nanotubes with attractive mechanical properties. J Eur Ceram Soc 2011;31:2691–8. doi:10.1016/j.jeurceramsoc.2010.11.009.

[15] Melk L, Roa Rovira JJ, García-Marro F, Antti ML, Milsom B, Reece MJ, et al. Nanoindentation and fracture toughness of nanostructured zirconia/multi-walled carbon nanotube composites. Ceram Int 2015;41:2453–61. doi:10.1016/j.ceramint.2014.10.060.

[16] Gallardo-López A, Morales-Rodríguez A, Vega-Padillo J, Poyato R, Muñoz A, Domínguez-Rodríguez A. Enhanced carbon nanotube dispersion in 3YTZP/SWNTs composites and its effect on room temperature mechanical and electrical properties. J Alloys Compd 2016;682:70–9. doi:10.1016/j.jallcom.2016.04.262.

[17] Lamnini S, Károly Z, Bódis E, Balázsi K, Balázsi C. Influence of structure on the

hardness and the toughening mechanism of the sintered 8YSZ/MWCNTs composites. Ceram Int 2018:0–1. doi:10.1016/j.ceramint.2018.11.207.

[18] INTERNATIONAL STANDARD Fine ceramics (advanced ceramics , advanced technical ceramics) — Test. Test 2008;2008.

[19] ISO18756:2003(E). Fine Ceramics (Advanced Ceramics, Advanced Technical Ceramics) — Determination of Fracture Toughness of Monolithic Ceramics at Room Temperature by The Surface Crack in Flexure (SCF) Method 2003;2005:1–36. doi:10.5594/J09750.

[20] Optaha Y, Normalisation OIDE. International standard 2015;2003.

[21] Nieto A, Zhao JM, Han YH, Hwang KH, Schoenung JM. Microscale tribological behavior and in vitro biocompatibility of graphene nanoplatelet reinforced alumina. vol. 61. Elsevier; 2016. doi:10.1016/j.jmbbm.2016.01.020.

[22] Lamnini S, Fogarassy Z, Horváth ZE, Tóth S, Balázsi K, Balázsi C. The role of the attrition milling on the grain sizeand distribution of the carbon nanotubesin YSZ powders. Bol La Soc Esp Ceram y Vidr 2018:1–8. doi:10.1016/j.bsecv.2018.10.001.

[23] Li H, Xie Y, Li K, Huang L, Huang S, Zhao B, et al. Ceram Int 2014. doi:10.1016/j.ceramint.2014.04.136.

[24] Zhang C, Nieto A, Agarwal A. Ultrathin graphene tribofilm formation during wear of Al_2O_3 –graphene composites. Nanomater Energy 2016;5:1–9. doi:10.1680/jnaen.15.00027.

Table1. Micro-structural properties of sintered 8YSZ/MWCNTs composites

Sample notation	**$MWCNT_S$ Content (wt %)**	**Apparent porosity (%)**	**Density ρ, (g/cm^3)**	**Average hardness *Hv*, (GPa)**	**Bending strength, (MPa)**	**Average toughness *Kc*, (MPa)**	**Grain size (μm)**
ZR	0	32.99	6.02	13.49±0.23	464	3.06±0.22	6.11±4.08
ZR-1	1	16.50	6.75	12.44±0.97	502	2.63±0.62	0.96±0.49
ZR-5	5	41.64	4.97	5.07±1.17	263	1.28±0.42	0.54±0.04
ZR-10	10	46.28	4.36	2.53±0.76	166	1.30±0.44	0.28±0.01

Table 2. Average arithmetic roughness measured inside and outside the wear track at *V1* and *V2* sliding speed.

Sample notation	**Roughness outside the track** ***Ra*, (μm)**	**Roughness inside the track via V1** ***Ra*, (μm)**	**Roughness inside the track via V2** ***Ra*, (μm)**
ZR	0.6	0.5	0.3
ZR-1	0.6	0.3	0.4
ZR-5	0.6	1.5	0.2
ZR-10	0.6	0.7	0.2

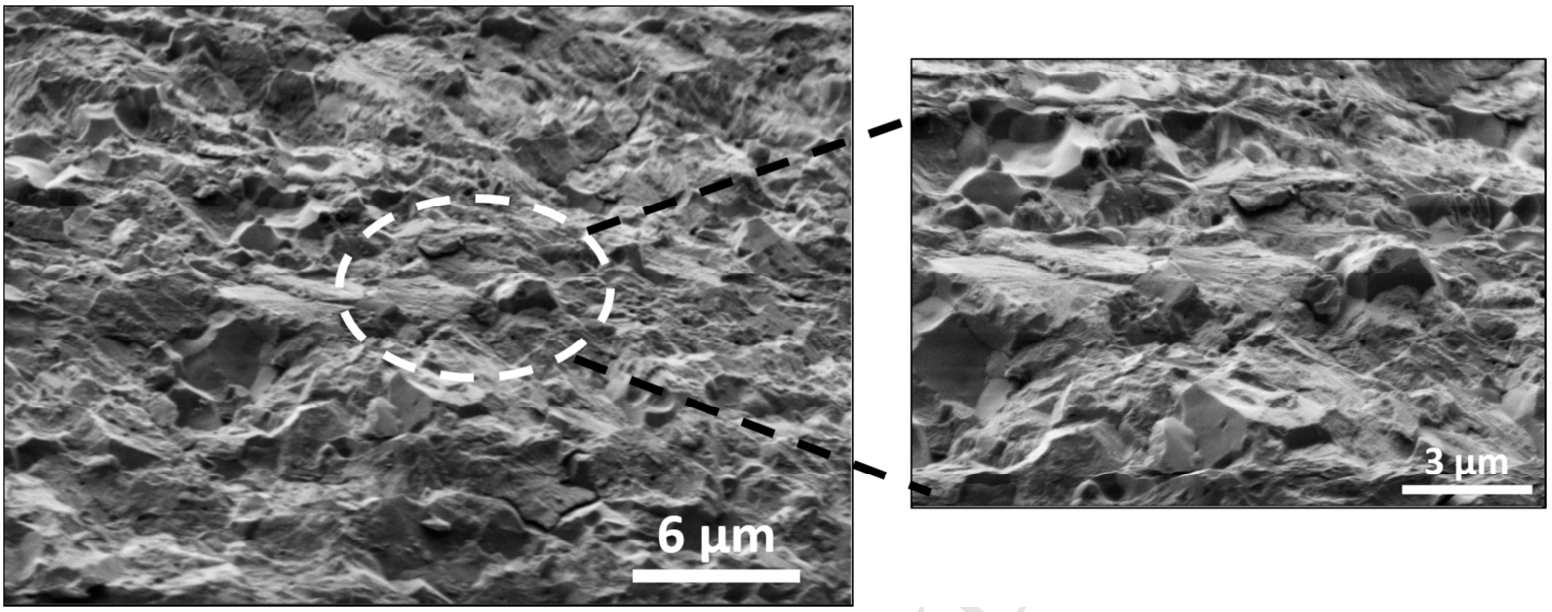

a)

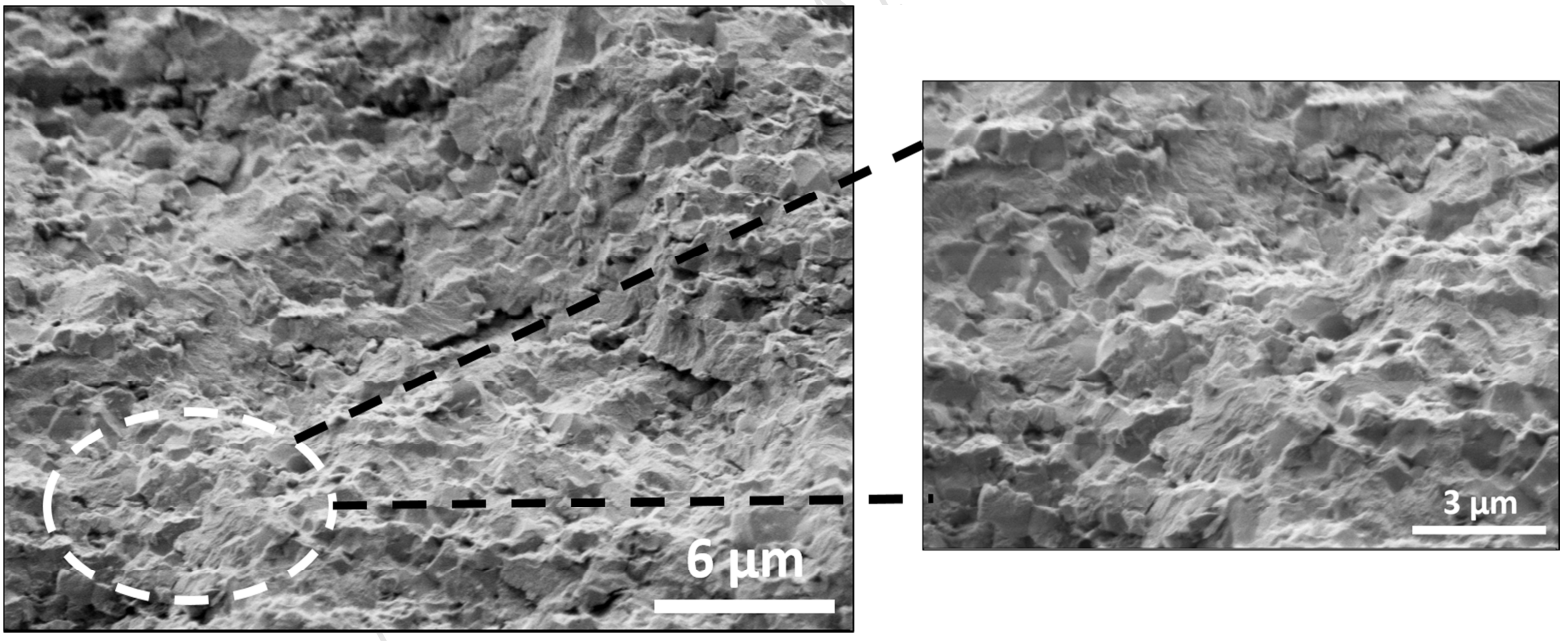

b)

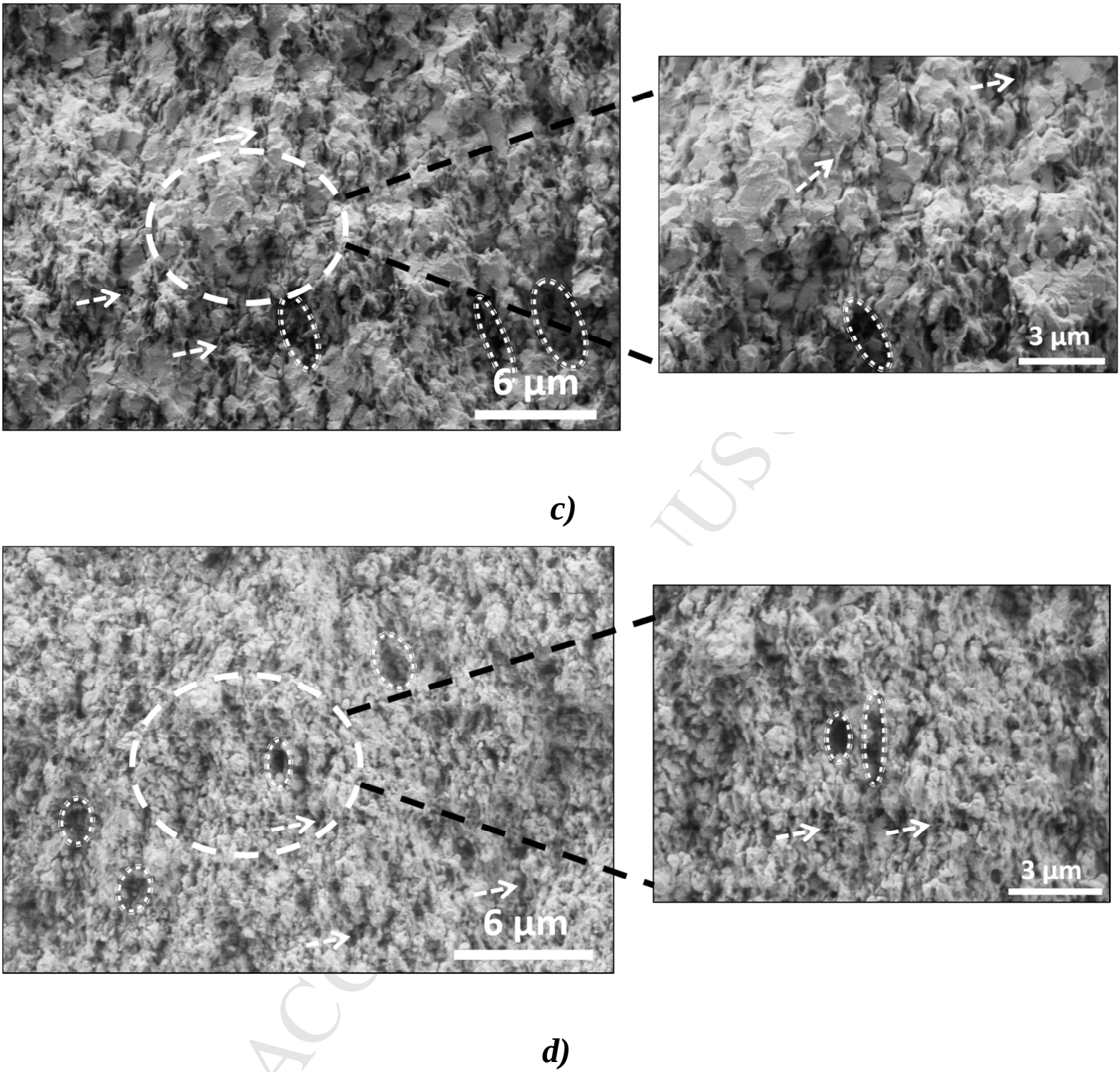

Fig. 1 *Fracture surfaces of ZR,* ZR-1, ZR-5 *and* ZR-10 *composites correspond to a), b), c) and d) respectively at different magnifications. In (c) & (d) the circles of dashed line mark microstructural defects generated by agglomerations and porosity in the grain boundaries, the arrows show MWCNTs fibers emplacement and dispersion in the microstructure.*

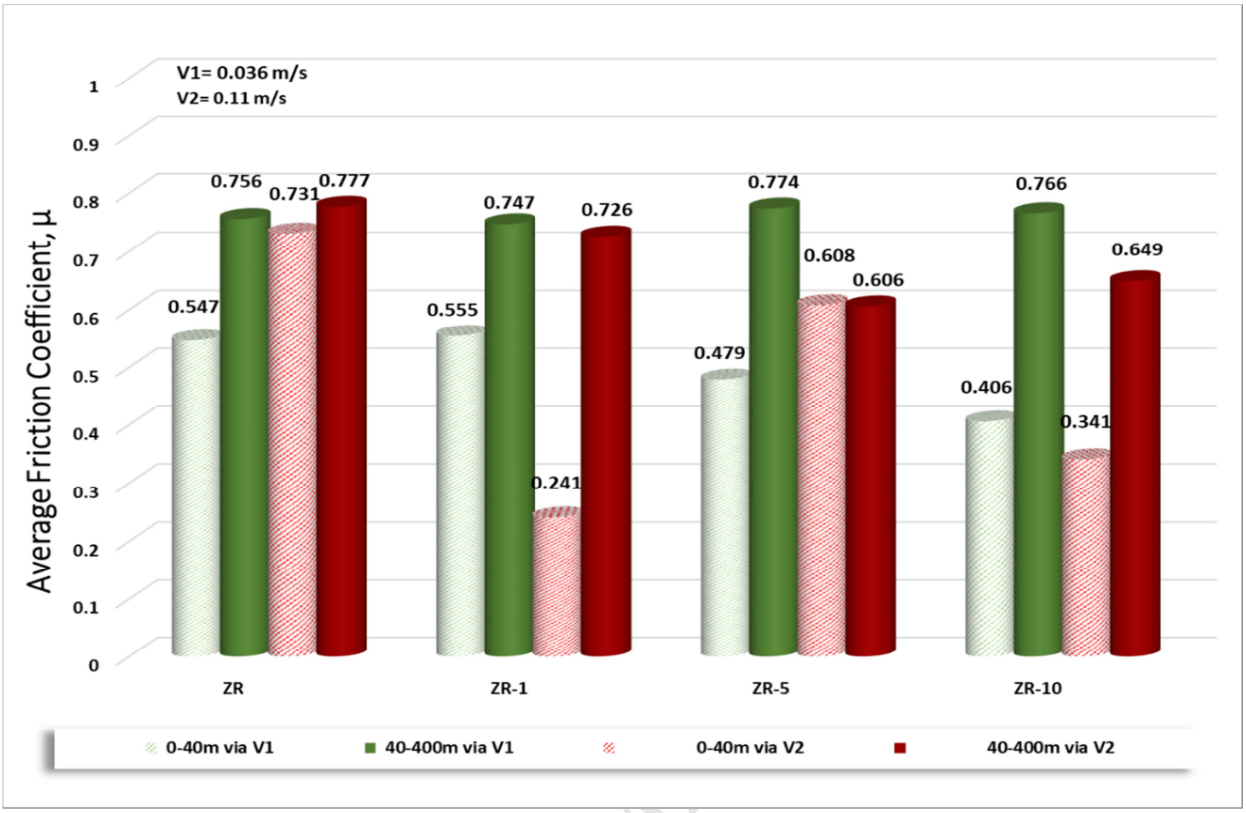

Fig. 2. *Comparative graph presenting the Average Friction Coefficient (μ) during transitory state (0-40m) and steady state (40-400m) for all the composites tested at fix normal load (5N) and different sliding rates (V1=0.036 m/s, V2=0.11 m/s).*

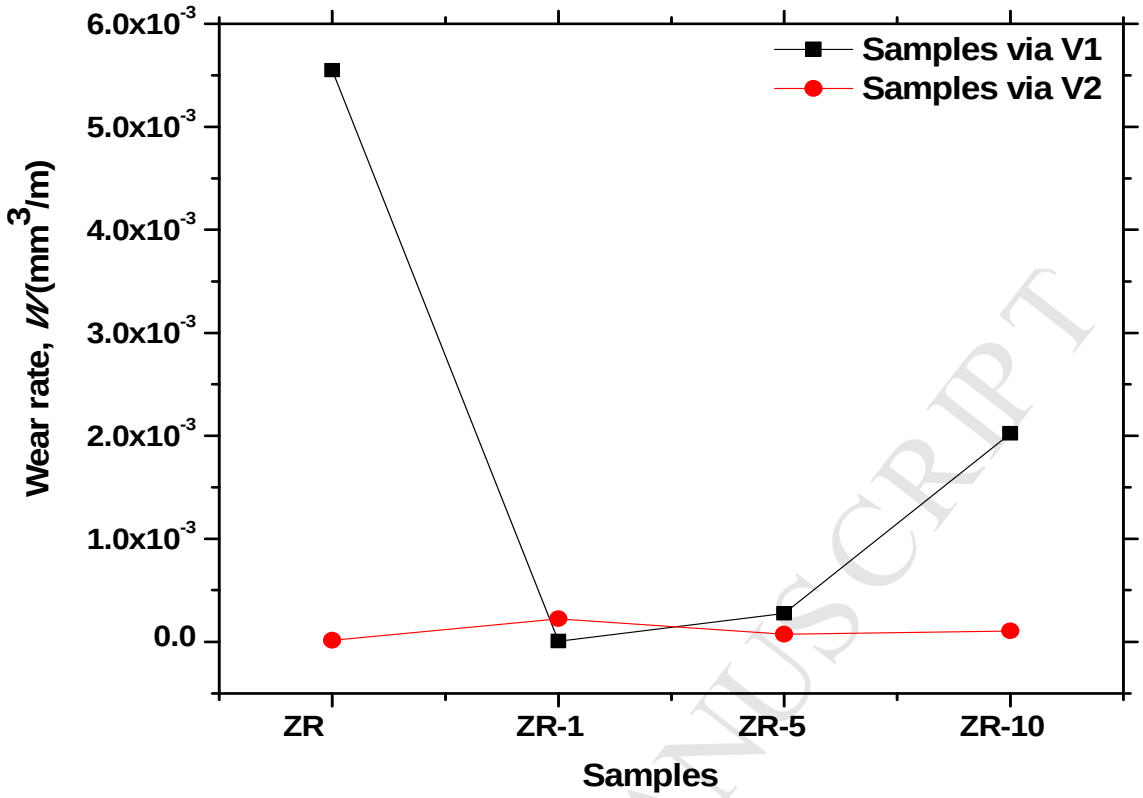

Fig. 3. *Wear rate (W) of the investigated composites via V1=0.036 m/s and V2=0.11 m/s sliding speed.*

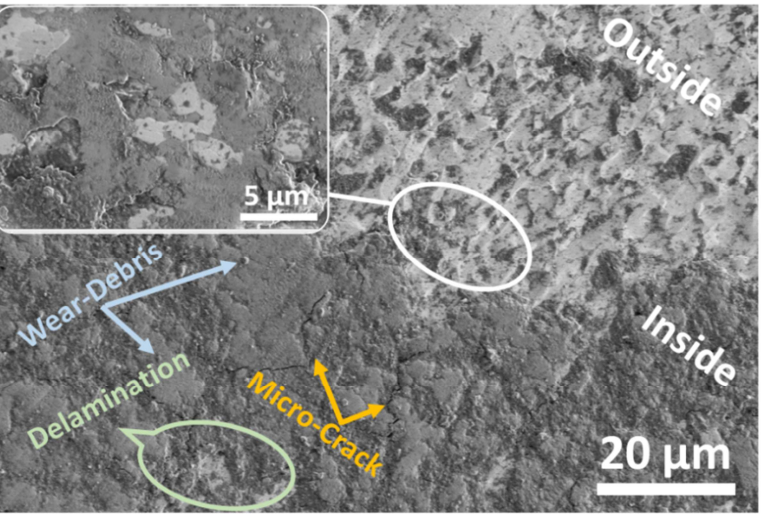
Outside
5 µm
Wear-Debris
Delamination
Micro-Crack
Inside
20 µm

a)

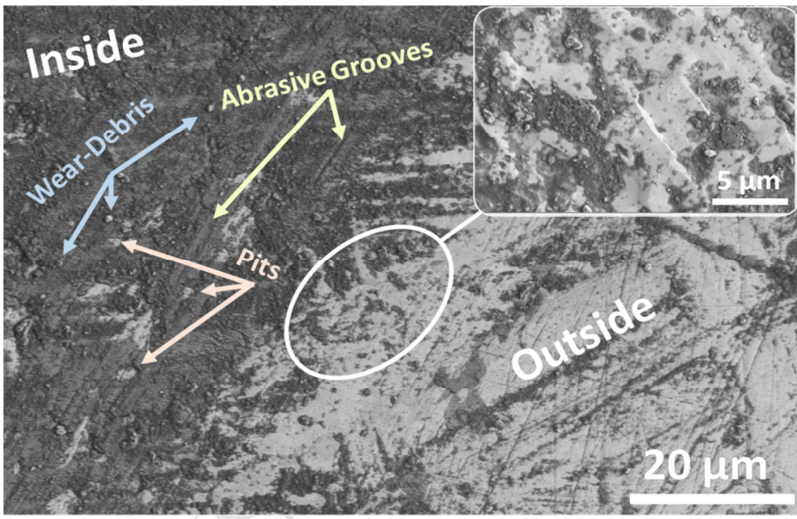
Inside
Wear-Debris
Abrasive Grooves
5 µm
Pits
Outside
20 µm

e)

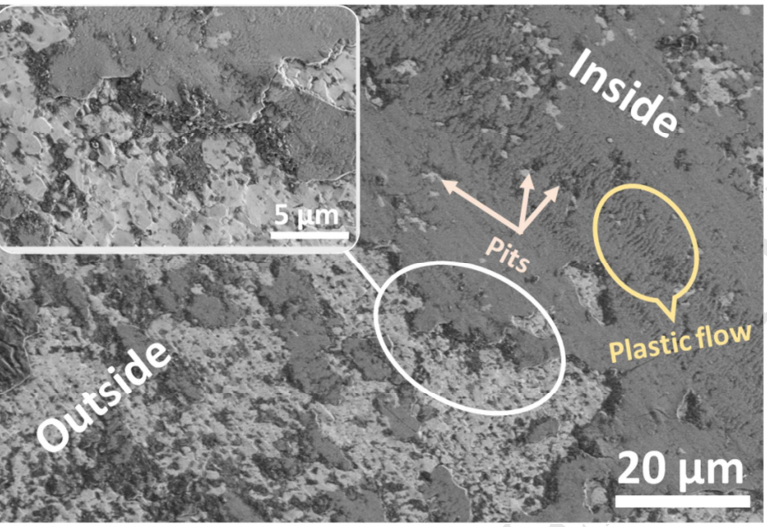
Inside
5 µm
Pits
Plastic flow
Outside
20 µm

b)

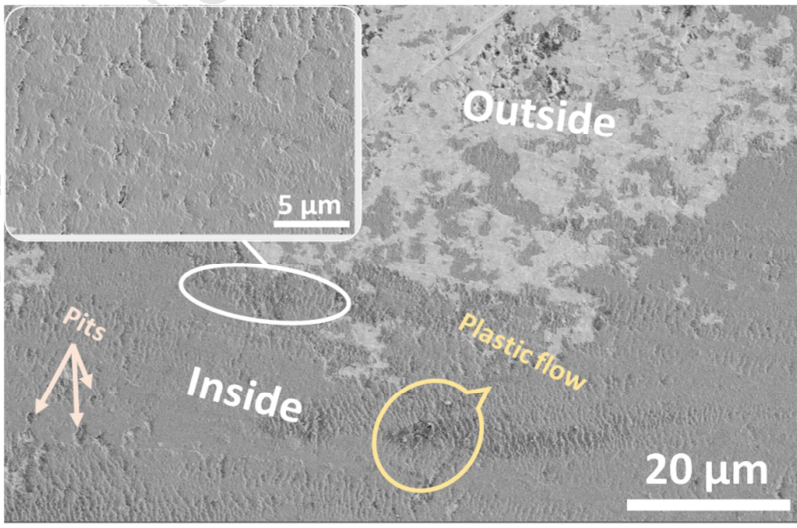
Outside
5 µm
Pits
Inside
Plastic flow
20 µm

f)

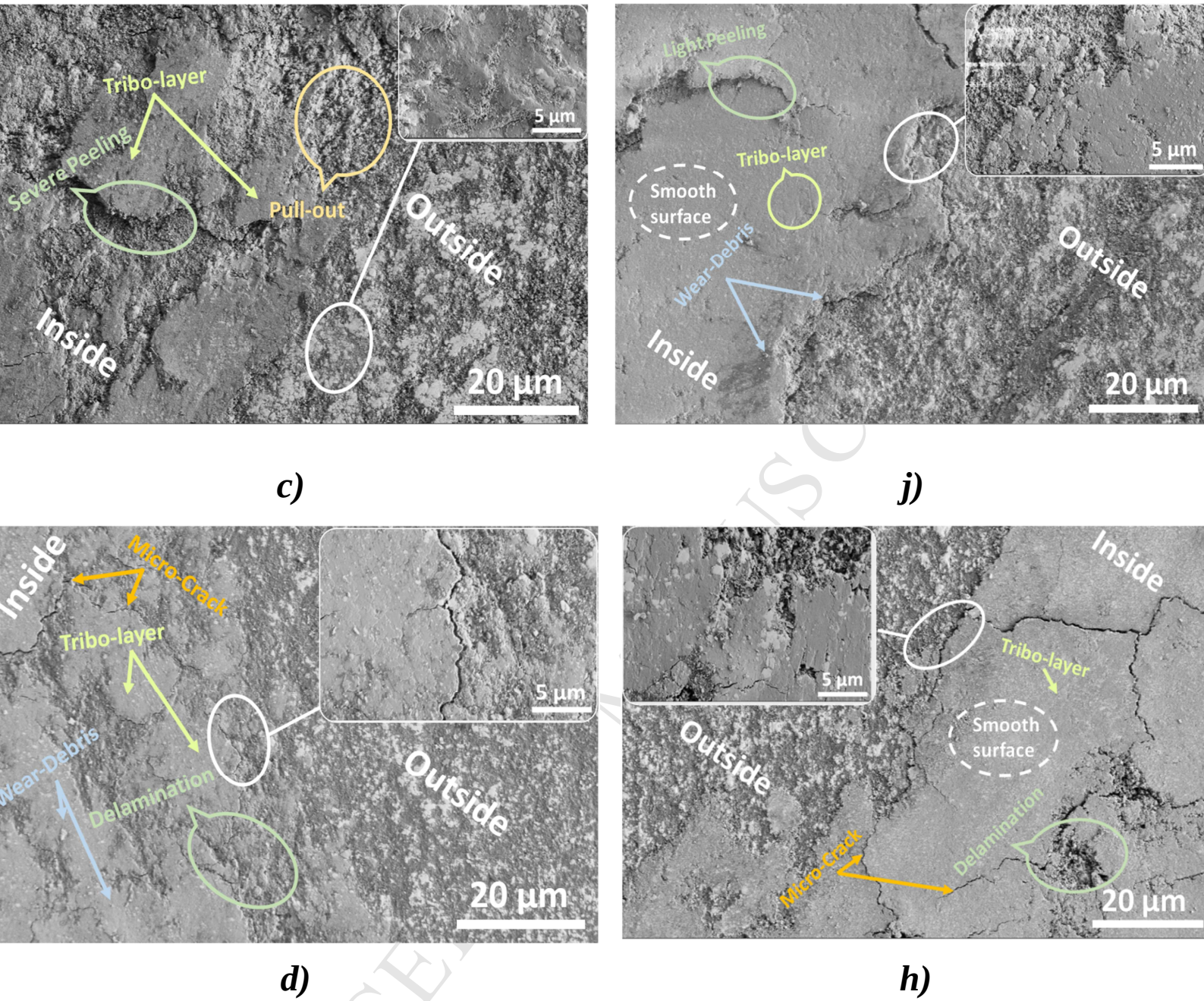

Fig. 4. *Comparative SEM micrographs inside and outside the wear track profileof ZR, ZR-1, ZR-5 and ZR-10 composites showing wear mechanism features and tribofilm formation during the test via V1=0.036 m/s correspond to a), b), c) and d), and via V2=0.11 m/s correspond to e), f), j) and h) respectively.*

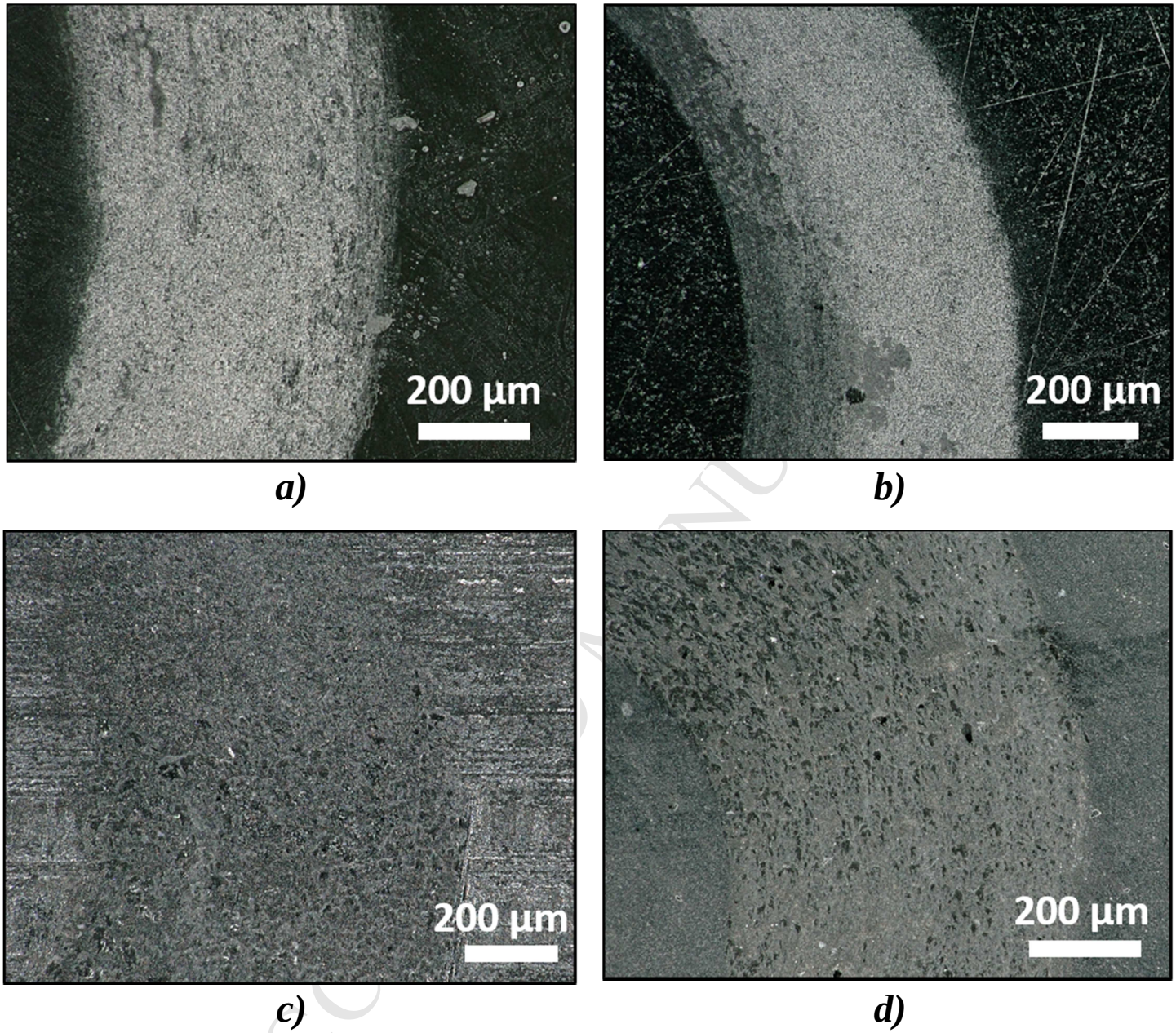

Fig. 5. *Keyence Digital microscope micrographs illustrating the increase in with after Tribo-test at V1=0.036 m/s sliding speed in ZR, ZR-1, ZR-5 and ZR-10 composites corresponding to a), b), c) and d) respectively.*

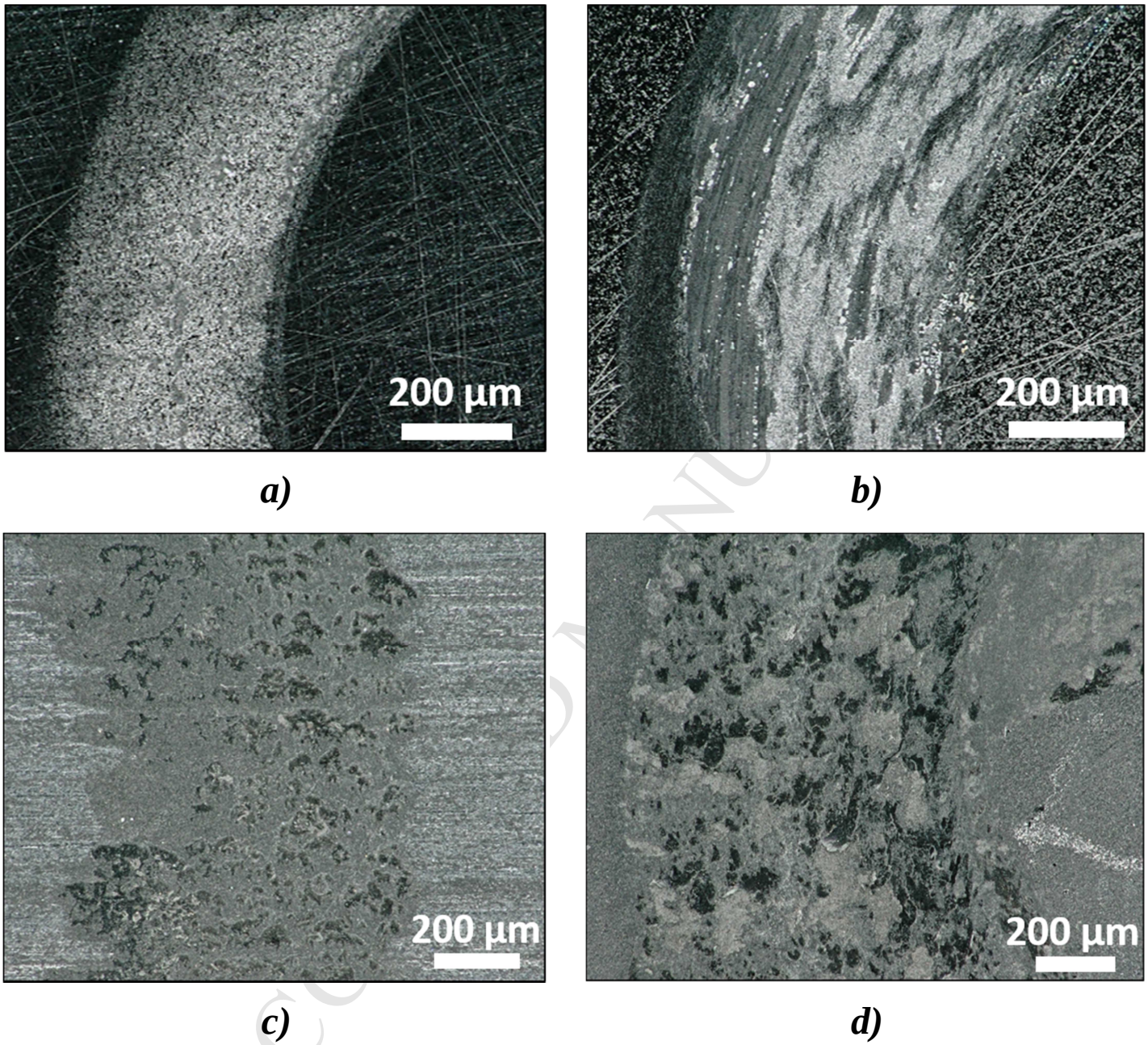

Fig. 6. *Keyence Digital microscope micrographs illustrating the increase in with after Tribo-test at V2=0.11 m/s sliding speed in ZR, ZR-1, ZR-5 and ZR-10 compositescorresponding to a), b), c) and d) respectively.*

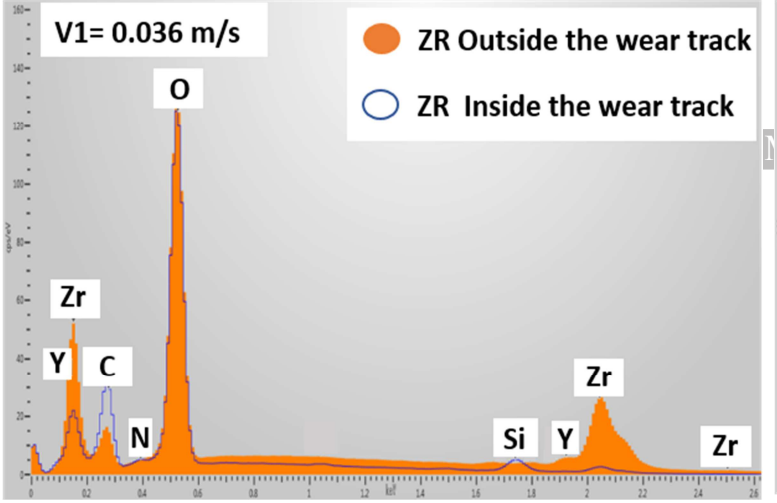
V1= 0.036 m/s
ZR Outside the wear track
ZR Inside the wear track
O
Zr
Y
C
N
Si
Y
Zr
Zr

a)

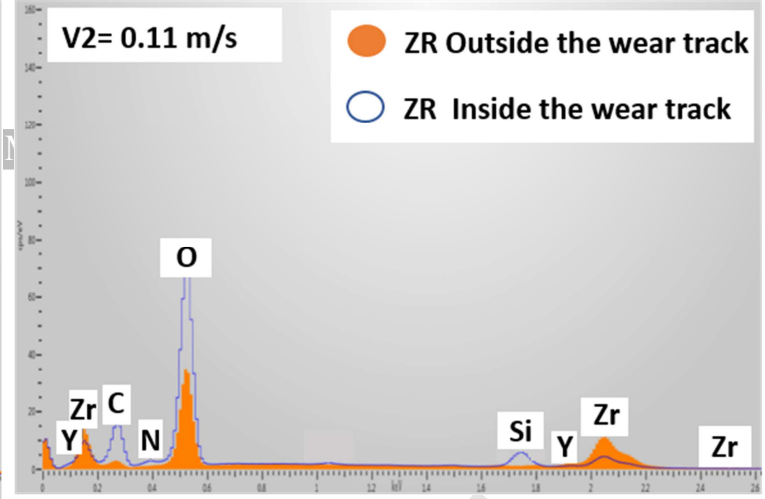
V2= 0.11 m/s
ZR Outside the wear track
ZR Inside the wear track
O
Zr
C
Y
N
Si
Y
Zr
Zr

e)

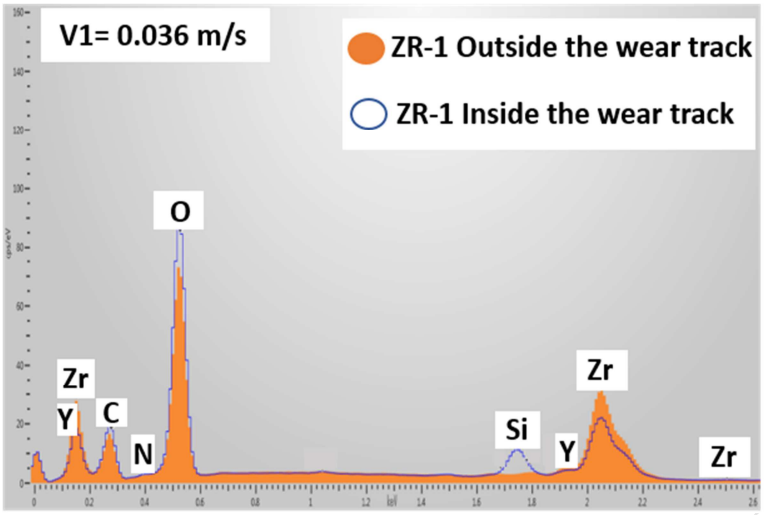
V1= 0.036 m/s
ZR-1 Outside the wear track
ZR-1 Inside the wear track
O
Zr
Y
C
N
Si
Y
Zr
Zr

b)

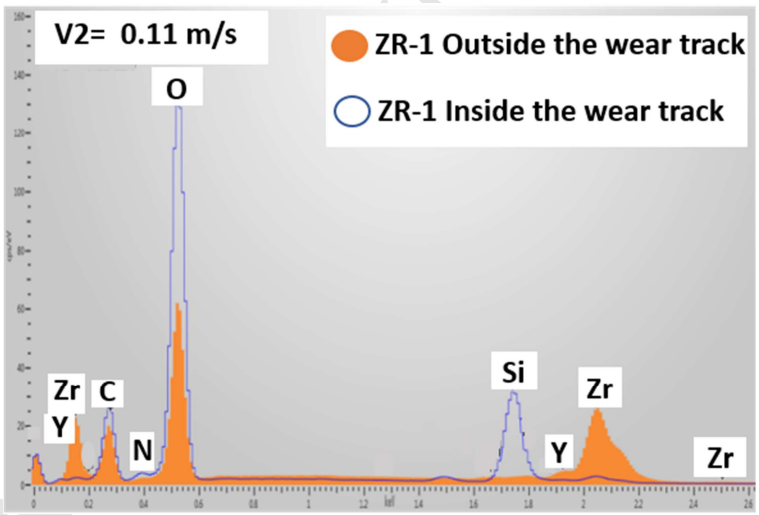
V2= 0.11 m/s
ZR-1 Outside the wear track
ZR-1 Inside the wear track
O
Zr
C
Y
N
Si
Y
Zr
Zr

f)

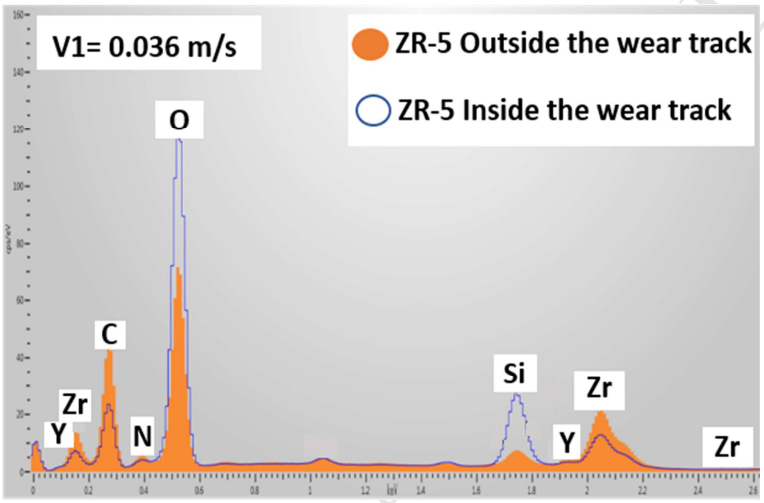
V1= 0.036 m/s
ZR-5 Outside the wear track
ZR-5 Inside the wear track
O
C
Zr
Y
N
Si
Y
Zr
Zr

c)

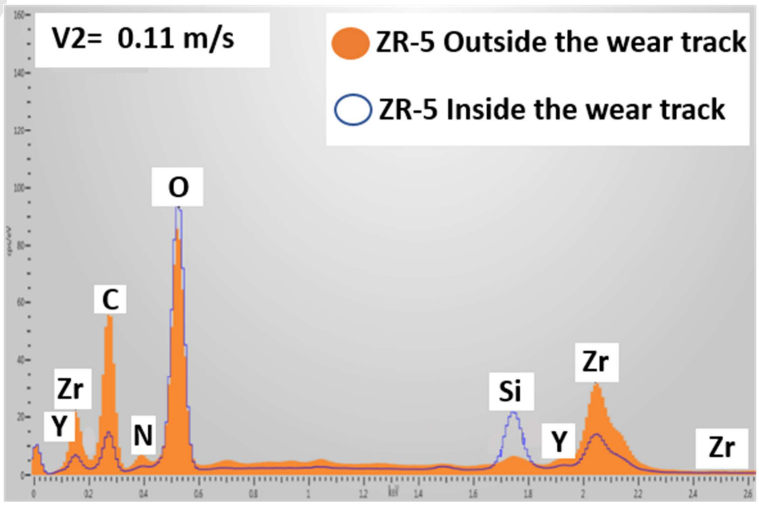
V2= 0.11 m/s
ZR-5 Outside the wear track
ZR-5 Inside the wear track
O
C
Zr
Y
N
Si
Y
Zr
Zr

j)

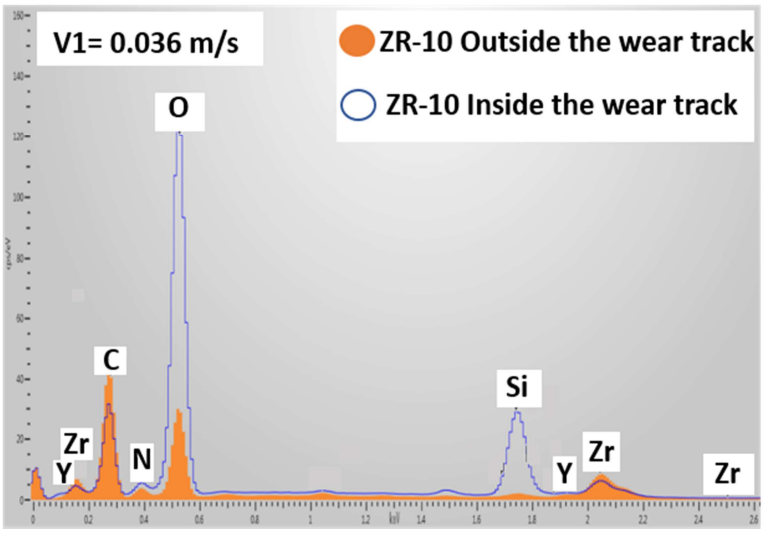

d)

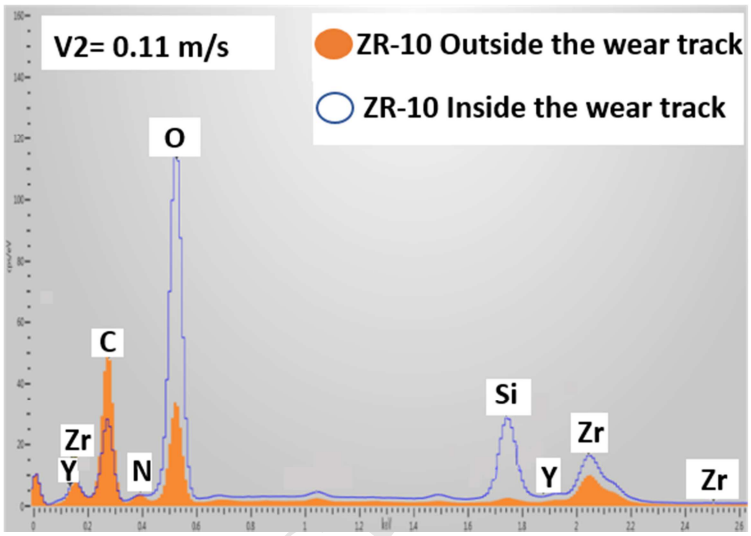

h)

Fig. 7. *Energy dispersive X-ray spectroscopy (EDS) inside and outside the wear track profile of ZR, ZR-1, ZR-5 and ZR-10 composites, tested via V1=0.036 m/s correspond to a), b), c) and d), and via V2=0.11 m/s correspond to e), f), j) and h) respectively*

Highlights

- outstanding wear improvement was reported with the addition of 1 wt% of MWCNTs
- at high sliding speed the wear rate results were not depending on MWCNTs content
- at high sliding speed the composite with high MWCNTs results in lower steady state μ
- carbon peak decrease is linked with MWCNTs exfoliation and intrinsic lubricant effect